

Two-pion interferometry for viscous hydrodynamic sources^{*}

Efaaf M. J.(安飞)¹ SU Zhong-Qian(苏中乾)¹ ZHANG Wei-Ning(张卫宁)^{1,2;1)}

¹ School of Physics and Optoelectronic Technology, Dalian University of Technology, Dalian 116024, China

² Department of Physics, Harbin Institute of Technology, Harbin 150006, China

Abstract: The space-time evolution of the (1+1)-dimensional viscous hydrodynamics with an initial quark-gluon plasma (QGP) produced in ultrarelativistic heavy ion collisions is studied numerically. The particle-emitting sources undergo a crossover transition from the QGP to hadronic gas. We take into account a usual shear viscosity for the strongly coupled QGP as well as the bulk viscosity which increases significantly in the crossover region. The two-pion Hanbury-Brown-Twiss (HBT) interferometry for the viscous hydrodynamic sources is performed. The HBT analyses indicate that the viscosity effect on the two-pion HBT results is small if only the shear viscosity is taken into consideration in the calculations. The bulk viscosity leads to a larger transverse freeze-out configuration of the pion-emitting sources, and thus increases the transverse HBT radii. The results of the longitudinal HBT radius for the source with Bjorken longitudinal scaling are consistent with the experimental data.

Key words: two-pion interferometry, viscous hydrodynamic sources, bulk viscosity, shear viscosity

PACS: 25.75.-q, 25.75.Gz, 25.75.Nq **DOI:** 10.1088/1674-1137/36/5/006

1 Introduction

The experimental results of the Relativistic Heavy Ion Collider (RHIC) at Brookhaven National Laboratory (BNL) indicate that the matter produced in the central collisions of Au+Au at $\sqrt{s_{NN}}=130$ and 200 GeV is a strongly coupled quark-gluon plasma (sQGP), and behaves like a perfect liquid [1]. Recently, the studies of the dissipative fluid dynamics have become a very hot topic in high energy heavy ion collisions [2–19], because people want to know why the sQGP exhibits an almost perfect fluid property and how to probe the viscosity effects on experimental observables.

The relativistic formulism of dissipative fluids was originally derived by Eckart [20] and Landau and Lifshitz [21]. Their theories contain only the first-order terms of the dissipative quantities and therefore are referred to as the first-order theories of dissipative fluids. The theories of dissipative fluids which include the terms up to the second order of the dissipative quantities were developed by Müller (non-

relativistic) [22] and Israel and Stewart (relativistic) [23]. These second-order theories can avoid the problem that sometimes the first-order theories may not satisfy causality. So they are also called the causal theories of dissipative fluids dynamics.

Although the Israel-Stewart second-order formalism for relativistic dissipative fluids [23] was established thirty years ago (in the 1970s), its numerical implementation in high energy heavy ion collisions begins in the 21st century. In Ref. [24], the viscous hydrodynamics based on the second-order theory is first used to study the system expansion in relativistic heavy ion collisions with the Bjorken scaling hypothesis [25]. Recently, the causal dissipative fluid dynamics has been used in high heavy ion collisions for investigations of the effects of shear viscosity [4–7, 10–15] and both shear and bulk viscosities [16–19] on the transverse momentum distribution [4–6, 11, 15–19], elliptic flow [5, 7, 10–18], and Hanbury-Brown-Twiss (HBT) interferometry [6, 18, 19].

As is well known, a dissipative fluid has not only

Received 31 August 2011

^{*} Supported by National Natural Science Foundation of China (11075027)

1) E-mail: wnzhang@dlut.edu.cn

©2012 Chinese Physical Society and the Institute of High Energy Physics of the Chinese Academy of Sciences and the Institute of Modern Physics of the Chinese Academy of Sciences and IOP Publishing Ltd

shear viscosity but also bulk viscosity. Recent research [16, 17] indicates that the effects of the shear and bulk viscosities on the elliptic flow are completely different in the RHIC heavy ion collisions. The shear viscosity suppresses the v_2 at larger transverse momenta but the bulk viscosity increases it [16, 17]. Unlike elliptic flow, which reflects the anisotropic pressure of the system, HBT correlations are related to the space-time structure of the particle-emitting source. Investigations of the shear and bulk viscosity effects on HBT interferometry may provide information about the shear and bulk viscosities from another point of view.

In the present work, we begin with the equations based on the Israel-Stewart theory for the net baryon free system formed in ultrarelativistic heavy ion collisions. For the central collisions, it is assumed that the system has Bjorken cylinder geometry (expanding isotropically in transverse and satisfying longitudinal boost-invariance) [26–28] and undergoes the crossover transition from the QGP to hadronic gas. We shall take into account both the shear and bulk viscosities and solve the viscous hydrodynamic equations by the relativistic Harten-Lax-Leer-Einfeldt (RHLE) algorithm [28–31]. By applying a simulated analysis of two-pion HBT interferometry [31, 32] to the (1+1)-dimensional viscous hydrodynamic sources, we investigate the effects of the shear and bulk viscosities on the HBT radii R_{out} , R_{side} , and R_{long} [33, 34]. The HBT analyses indicate that the viscosity effect on the HBT results is small if one considers only the shear viscosity. The bulk viscosity leads to a larger transverse freeze-out configuration of the pion sources, and thus increases the transverse HBT radii. The results of the longitudinal HBT radius for the source with Bjorken longitudinal scaling are consistent with the experimental data.

This paper is organized as follows. In Sec. 2, we review briefly the evolution equations of the relativistic dissipative fluid dynamics for the net baryon free system with Bjorken cylinder geometry. We present the expressions of the relaxation equations for the shear tensor and bulk pressure for the system considered. The detailed derivations are given in Appendix A. In Sec. 3, we discuss the numerical algorithm for solving the viscous hydrodynamics. The equations of state and initial conditions used in our calculations are outlined. We present our numerical results of the viscous and ideal fluid evolutions. In Sec. 4, we perform the two-pion HBT interferometry for the viscous hydrodynamic sources. We investigate the viscosity

effects on the HBT radii for the viscous hydrodynamic sources with only shear viscosity and with both shear and bulk viscosities. We also investigate the HBT results for the viscous sources with lower and higher freeze-out temperatures and initial energy densities. Finally, a conclusion is given in Sec. 5.

2 Equations of relativistic dissipative fluid dynamics

First, we briefly review the evolution equations of relativistic dissipative fluid dynamics for a system with Bjorken-cylinder geometry and zero net baryon density. The basic equations can be referred to [2–4, 8, 35].

The evolution equations of hydrodynamics come from physics conservations. For the baryon free system, we consider only the energy-momentum conservation in the hydrodynamics. It is convenient to describe the Bjorken-cylinder system with the coordinates (τ, ρ, ϕ, η) , where $\tau = \sqrt{t^2 - z^2}$ is the longitudinal proper time, ρ and ϕ are the polar coordinates in the plane transverse to the beam direction z , and $\eta = \frac{1}{2} \ln[(t+z)/(t-z)]$ is the space-time rapidity. The metric tensors $g^{\mu\nu}$ and $g_{\mu\nu}$ are expressed in the frame of these curvilinear space-time coordinates as

$$g^{\mu\nu} = \text{diag}(1, -1, -1/\rho^2, -1/\tau^2), \quad (1)$$

$$g_{\mu\nu} = \text{diag}(1, -1, -\rho^2, -\tau^2).$$

Some notations used in this paper are

$$d_\mu u^\nu \equiv \partial_\mu u^\nu + \Gamma_{\alpha\mu}^\nu u^\alpha, \quad (2)$$

$$\Gamma_{\alpha\beta}^\gamma \equiv \frac{1}{2} g^{\gamma\sigma} (\partial_\alpha g_{\beta\sigma} + \partial_\beta g_{\sigma\alpha} - \partial_\sigma g_{\alpha\beta}), \quad (3)$$

$$\Theta \equiv d_\mu u^\mu, \quad D \equiv u^\mu d_\mu, \quad (4)$$

$$\nabla^\mu \equiv \Delta^{\mu\nu} d_\nu, \quad (5)$$

$$\Delta^{\mu\nu} \equiv g^{\mu\nu} - u^\mu u^\nu, \quad (6)$$

$$\nabla^{(\mu} u^{\nu)} \equiv \nabla^{(\mu} u^{\nu)} - \frac{1}{3} \Delta^{\mu\nu} d_\lambda u^\lambda, \quad (7)$$

$$A^{(\alpha\beta)} \equiv (A^{\alpha\beta} + A^{\beta\alpha})/2, \quad (8)$$

where d_μ denotes the covariant derivative, $\partial_\alpha = \partial/\partial x^\alpha$ and $u^\mu = \gamma(1, \mathbf{v})$ are the 4-derivative and 4-velocity ($\gamma = 1/\sqrt{1-\mathbf{v}^2}$), $\Gamma_{\alpha\beta}^\gamma$ is the Christoffel symbol, and $A^{(\alpha\beta)}$ denotes the symmetrization of the quantity $A^{\alpha\beta}$.

We adopt the Landau and Lifshitz frame [21] in

which the local energy flow is zero. The energy-momentum tensor of a fluid cell in relativistic dissipative hydrodynamics is

$$T^{\mu\nu} = \varepsilon u^\mu u^\nu - (p + \Pi) \Delta^{\mu\nu} + \pi^{\mu\nu}, \quad (9)$$

where, ε is the energy density, p is the local isotropic pressure, Π is the bulk viscosity pressure, and $\pi^{\mu\nu}$ is the shear stress tensor. Using the covariant derivative form, the energy-momentum conservation can be reexpressed as

$$d_\mu T^{\mu\nu} \equiv \partial_\mu T^{\mu\nu} + \Gamma_{\mu\lambda}^\mu T^{\lambda\nu} + T^{\mu\lambda} \Gamma_{\lambda\mu}^\nu = 0. \quad (10)$$

For the Bjorken cylinder, the longitudinal velocity is given by $v^z = z/t$ and the hydrodynamical solution at an arbitrary longitudinal coordinate z can be obtained by the Lorentz boost with the rapidity $\eta = \tanh^{-1}(z/t)$ from the system's transverse evolution at $z = 0$ [26–28, 36]. So we need only solve the hydrodynamical equations at $z = 0$ ($\eta = 0$) in this case. Considering $u^\eta = 0$ at $z = 0$ and assuming $u^\phi = 0$, Eq. (10) becomes

$$\begin{cases} \partial_\tau T^{\tau\tau} + \partial_\rho T^{\rho\tau} + \Gamma_{\eta\eta}^\tau T^{\eta\eta} + \Gamma_{\eta\tau}^\eta T^{\tau\tau} + \Gamma_{\phi\rho}^\phi T^{\rho\tau} = 0, \\ \partial_\tau T^{\tau\rho} + \partial_\rho T^{\rho\rho} + \Gamma_{\phi\phi}^\rho T^{\phi\phi} + \Gamma_{\phi\rho}^\phi T^{\rho\rho} + \Gamma_{\eta\tau}^\eta T^{\tau\rho} = 0. \end{cases} \quad (11)$$

Introducing the quantities

$$\mathcal{P}_\rho = p + \Pi + \pi^{\rho\rho}/\gamma^2, \quad (12)$$

$$\mathcal{P}_\phi = p + \Pi + \pi^{\phi\phi}\rho^2, \quad (13)$$

$$\mathcal{P}_\eta = p + \Pi + \pi^{\eta\eta}\tau^2, \quad (14)$$

$$E = (\varepsilon + \mathcal{P}_\rho)\gamma^2 - \mathcal{P}_\rho, \quad (15)$$

$$M = (E + \mathcal{P}_\rho)v_\rho, \quad (16)$$

the non zero components of the energy-momentum tensor $T^{\mu\nu}$ can be expressed as

$$T^{\tau\tau} = E, \quad T^{\tau\rho} = T^{\rho\tau} = M, \quad (17)$$

$$T^{\rho\rho} = Mv_\rho + \mathcal{P}_\rho, \quad (18)$$

$$T^{\phi\phi} = \frac{\mathcal{P}_\phi}{\rho^2}, \quad T^{\eta\eta} = \frac{\mathcal{P}_\eta}{\tau^2}, \quad (19)$$

and, Eq. (11) can be rewritten as

$$\begin{aligned} \partial_\tau E + \partial_\rho [(E + \mathcal{P}_\rho)v_\rho] &= -(E + \mathcal{P}_\rho) \left(\frac{v_\rho}{\rho} + \frac{1}{\tau} \right) \\ &+ \frac{(\mathcal{P}_\rho - \mathcal{P}_\eta)}{\tau}, \end{aligned} \quad (20)$$

$$\begin{aligned} \partial_\tau M + \partial_\rho (Mv_\rho + \mathcal{P}_\rho) &= -M \left(\frac{v_\rho}{\rho} + \frac{1}{\tau} \right) \\ &- \frac{(\mathcal{P}_\rho - \mathcal{P}_\phi)}{\rho}. \end{aligned} \quad (21)$$

The coupled Eqs. (20) and (21) are the evolution equations of the dissipative hydrodynamics for the Bjorken cylinder system, which can be numerically solved by the RHLLE algorithms [28–31]. The quantities \mathcal{P}_ρ , \mathcal{P}_ϕ , and \mathcal{P}_η include the effects of dissipation and they reduce to the isotropic pressure p for perfect fluids.

Next, we present the relaxation equations that the dissipation quantities ($\pi^{\mu\nu}$ and Π) are satisfied for our system. The detailed derivations of the relaxation equations are given in Appendix A. In order to obtain the system evolution we need to solve the Eqs. (20) and (21) together with the relaxation equations.

In the Landau and Lifshitz frame and for the baryon free system, the dissipative effect from the heat conduction can be neglected [2, 3, 5, 10, 11]. On the other hand, one can also ignore the effect of vorticity because it is small for the longitudinally boost-invariant system [7, 12, 13]. In this case, the relaxation equations for the shear tensor $\pi^{\mu\nu}$ and bulk pressure Π can be written as [2–4, 8, 35]

$$\begin{aligned} &\tau_\pi \Delta^{\mu\alpha} \Delta^{\nu\beta} D\pi_{\alpha\beta} + \pi^{\mu\nu} \\ &= 2\tilde{\eta} \nabla^{\langle\mu} u^{\nu\rangle} - \frac{1}{2} \pi^{\mu\nu} \tilde{\eta} T d_\lambda \left(\frac{\tau_\pi u^\lambda}{\tilde{\eta} T} \right), \end{aligned} \quad (22)$$

$$\begin{aligned} &\tau_\Pi D\Pi + \Pi \\ &= -\tilde{\zeta} d_\mu u^\mu - \frac{1}{2} \Pi \tilde{\zeta} T d_\lambda \left(\frac{\tau_\Pi u^\lambda}{\tilde{\zeta} T} \right), \end{aligned} \quad (23)$$

where, $\tilde{\eta}$ and $\tilde{\zeta}$ denote the shear and bulk viscous coefficients, $\tau_\pi = 2\beta_2 \tilde{\eta}$ and $\tau_\Pi = \beta_0 \tilde{\zeta}$ are the corresponding relaxation times, β_2 and β_0 are the relaxation coefficients for the expansion of entropy flow up to the second-order of the dissipative quantities, and T is the temperature.

For the symmetric Bjorken cylinder and at $z = 0$ ($u^\phi = u^\eta = 0$), Eqs. (22) and (23) can be written in forms that are suitable for solving numerically as for (detailed derivations, see Appendix A)

$$\begin{aligned} \frac{\partial}{\partial \tau} \tau^{\rho\rho} + v_\rho \frac{\partial \tau^{\rho\rho}}{\partial \rho} &= \frac{1}{\gamma \tau_\pi} (-\tau^{\rho\rho} + 2\tilde{\eta} \sigma^{\rho\rho}) \\ &- \frac{\tau^{\rho\rho}}{2\gamma} \left[\Theta + \frac{\tilde{\eta} T}{\tau_\pi} D \left(\frac{\tau_\pi}{\tilde{\eta} T} \right) \right], \end{aligned} \quad (24)$$

$$\frac{\partial}{\partial \tau} \tau^{\phi\phi} + v_\rho \frac{\partial \tau^{\phi\phi}}{\partial \rho} = \frac{1}{\gamma \tau_\pi} (-\tau^{\phi\phi} + 2\tilde{\eta} \sigma^{\phi\phi}) - \frac{\tau^{\phi\phi}}{2\gamma} \left[\Theta + \frac{\tilde{\eta} T}{\tau_\pi} D \left(\frac{\tau_\pi}{\tilde{\eta} T} \right) \right], \quad (25)$$

$$\frac{\partial}{\partial \tau} \tau^{\eta\eta} + v_\rho \frac{\partial \tau^{\eta\eta}}{\partial \rho} = \frac{1}{\gamma \tau_\pi} (-\tau^{\eta\eta} + 2\tilde{\eta} \sigma^{\eta\eta}) - \frac{\tau^{\eta\eta}}{2\gamma} \left[\Theta + \frac{\tilde{\eta} T}{\tau_\pi} D \left(\frac{\tau_\pi}{\tilde{\eta} T} \right) \right], \quad (26)$$

$$\frac{\partial}{\partial \tau} \Pi + v_\rho \frac{\partial \Pi}{\partial \rho} = \frac{1}{\gamma \tau_\Pi} (-\Pi - \tilde{\zeta} \Theta) - \frac{\Pi}{2\gamma} \left[\Theta + \frac{\tilde{\zeta} T}{\tau_\Pi} D \left(\frac{\tau_\Pi}{\tilde{\zeta} T} \right) \right], \quad (27)$$

where $\tau^{\rho\rho}$, $\tau^{\phi\phi}$, and $\tau^{\eta\eta}$ are three introduced quantities with relations to the nonzero components of $\pi^{\mu\nu}$ as

$$\pi^{\mu\nu} = \begin{pmatrix} \gamma^2 v_\rho^2 \tau^{\rho\rho} & \gamma^2 v_\rho \tau^{\rho\rho} & 0 & 0 \\ \gamma^2 v_\rho \tau^{\rho\rho} & \gamma^2 \tau^{\rho\rho} & 0 & 0 \\ 0 & 0 & \rho^{-2} \tau^{\phi\phi} & 0 \\ 0 & 0 & 0 & \tau^{-2} \tau^{\eta\eta} \end{pmatrix}, \quad (28)$$

where

$$\tau^{\rho\rho} + \tau^{\phi\phi} + \tau^{\eta\eta} = 0, \quad (29)$$

from the traceless condition $\pi^\mu_\mu = 0$ [4, 24]. In Eqs. (24)–(27),

$$\begin{aligned} \Theta &= d_\mu u^\mu = \frac{\partial \gamma}{\partial \tau} + \frac{\partial(\gamma v_\rho)}{\partial \rho} + \gamma \left(\frac{v_\rho}{\rho} + \frac{1}{\tau} \right) \\ &\equiv \theta + \gamma \left(\frac{v_\rho}{\rho} + \frac{1}{\tau} \right), \end{aligned} \quad (30)$$

$$\sigma^{\rho\rho} = \left(-\theta + \frac{1}{3} \Theta \right), \quad (31)$$

$$\sigma^{\phi\phi} = \left(\frac{-\gamma v_\rho}{\rho} + \frac{1}{3} \Theta \right), \quad (32)$$

$$\sigma^{\eta\eta} = \left(\frac{-\gamma}{\tau} + \frac{1}{3} \Theta \right), \quad (33)$$

and $D = u^\mu d_\mu$ reduce to $\gamma(\partial_\tau + v_\rho \partial_\rho)$.

When performing numerical calculations we need to solve the evolution Eqs. (20) and (21) and the relaxation Eqs. (24)–(27) simultaneously. For the sQGP, the ratio of the shear viscosity to the entropy density satisfies $\tilde{\eta}/s \gtrsim 1/4\pi$ [37–39], and the ratio of the bulk-to-shear viscosities is proportional to the deviation of the sound velocity square from that of the

ideal hadronic gas, $\tilde{\zeta}/\tilde{\eta} \simeq -\kappa(v_s^2 - 1/3)$ [17, 40–42]. Based on the calculations of the $\mathcal{N} = 2^*$ gauge theory, the value of κ is between 3.142 and 4.935 [41]. In our calculations we take $\tilde{\eta}/s = 2C_s(1/4\pi)$ ($C_s = 1, 2$) and $\kappa = 4.75$. The relaxation times for the shear and bulk viscosities are taken as $\tau_\pi = \frac{6\tilde{\eta}}{sT}$ and $\tau_\Pi = \tau_\pi$ as in Refs. [6, 10, 12, 15, 17, 18, 23] for simplicity.

3 Numerical solution of viscous hydrodynamics

When solving the viscous hydrodynamic equations numerically, we encounter the following two types of equations:

$$\partial_\tau U + \partial_\rho F(U) = G(U) \quad (34)$$

and

$$\partial_\tau U + v_\rho \partial_\rho F(U) = G(U). \quad (35)$$

For the evolution Eqs. (20) and (21), U in Eq. (34) can be replaced by E or M , and for the relaxation Eqs. (24)–(27), U in Eq. (35) can be replaced by $\tau^{\rho\rho}$, $\tau^{\phi\phi}$, $\tau^{\eta\eta}$, or Π . Eq. (34) can be solved directly by the RHLLE algorithm [28–31]. For Eq. (35) we can change it to the type of Eq. (34) by adding the term $F(U) \partial_\rho v_\rho$ to both sides of the equation, and then solve it with the RHLLE algorithm. In the calculations, we solve simultaneously the six coupled equations of (20), (21), and (24)–(27) for the quantities ($E, M, \tau^{rr}, \tau^{\phi\phi}, \tau^{\eta\eta}, \Pi$) at each time step. The width of a time step is taken to be $\Delta\tau = 0.04$ fm/ c and the width of a space step is taken to be $0.99\Delta\tau$ fm. The set of the coupled Eqs. (20), (21), and (24)–(27) is closed by the equation of state (EOS), and the transverse velocity and local energy density satisfy

$$v_\rho = \frac{M}{E + P_\rho}, \quad \varepsilon = E - \frac{M^2}{E + P_\rho}. \quad (36)$$

The EOS used in the calculations is the parametric EOS which combines a hadron resonance gas at low temperatures with lattice QCD at high temperatures [43]. Fig. 1(a) shows the energy density ε and pressure p as functions of temperature. Fig. 1(b) shows the square of sound velocity v_s^2 and the difference between ε and $3p$, $\Delta = \varepsilon - 3p$, as functions of temperature. The transition temperature T_c is taken to be 170 MeV.

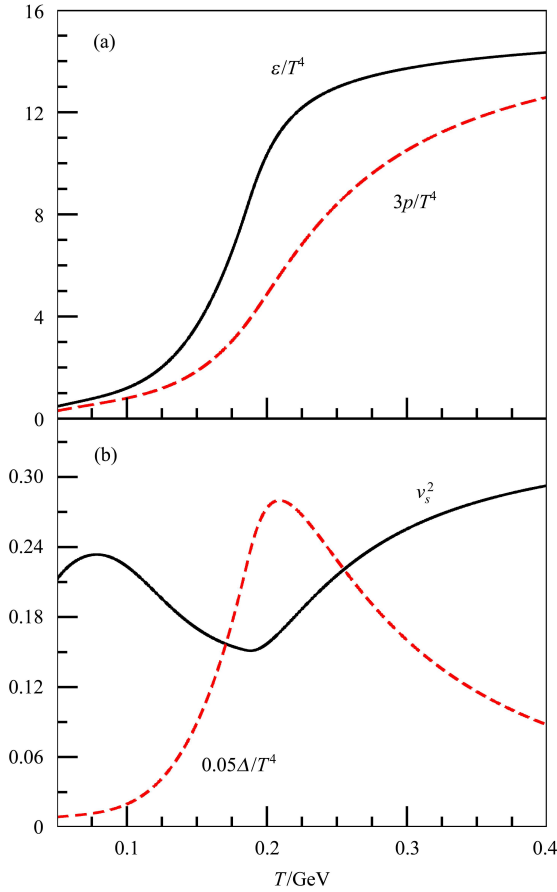


Fig. 1. (color online) (a) The energy density ε and pressure p as functions of temperature. (b) The square of sound velocity v_s^2 and the difference $\Delta = \varepsilon - 3p$ as functions of temperature.

On the basis of the Bjorken picture [25], the system evolves hydrodynamically after a proper time τ_0 . In our calculations, we take the initial time $\tau_0 = 0.6$ fm/c, and use a Gaussian initial transverse distribution of energy density at $z = 0$,

$$\varepsilon(\rho, z = 0) = \varepsilon_0 \exp(-\rho^2/2\sigma_0), \quad (37)$$

where ε_0 is taken to be 30 GeV/fm³ and σ_0 is taken to be 3.3 fm. The initial shear tensor components are taken to be

$$\tau^{\rho\rho}(\rho) = \tau^{\phi\phi}(\rho) = \frac{\varepsilon(\rho)}{18}$$

and

$$\tau^{\eta\eta}(\rho) = -\frac{\varepsilon(\rho)}{9}$$

as in Ref. [2]. We find that the system evolution is almost independent of the initial value of the bulk pressure because it is almost zero at the initial temperature, which is much higher than T_c . So we take the initial bulk pressure to be zero in the calculations.

Figures 2(a) and (b) show the temperature and transverse velocity profiles in the $z = 0$ plane for the viscous fluid with only shear viscosity ($C_s = 2$). Correspondingly, Figs. 2(c) and (d) show the temperature and transverse velocity profiles in the $z = 0$ plane for the fluid with shear and bulk viscosities. In Fig. 2, the dashed lines are for the ideal fluid for comparison, and the time $t_0 = \tau_0$, $t_n = \tau_0 + 2^n(20\Delta\tau)$ ($n = 1, 2, 3, 4$, $\Delta\tau = 0.04$ fm/c). For the only shear viscosity case, the viscous fluids cool a little more slowly than the ideal fluid for small time, and the transverse velocities of the viscous fluid are higher than the corresponding velocities of ideal fluid. Once the bulk viscosity is taken into account, one can see that the viscous fluid cools more slowly and its transverse velocities are lower than the corresponding velocities of ideal fluid. This is because the bulk viscosity decreases the system pressure (see Eq. (9) and notice $\Pi < 0$) and therefore decreases the gradient of the pressures in and out of the system.

In Fig. 3, we show the ratios of the viscosity quantities $\tau^{\rho\rho}$, $\tau^{\phi\phi}$, $\tau^{\eta\eta}$, and Π to the central initial energy density ε_0 , as functions of the transverse coordinate and time for the viscous fluid ($C_s = 2$). In Fig. 4, we draw the isotherms for the viscous ($C_s = 2$) and ideal fluids in the $z = 0$ plane. It can be seen that the contours for the shear-only viscous fluid are slightly larger than those of the ideal fluid, and the bulk viscosity lets the contours of the viscous fluid be much larger than those of the ideal fluid. This is consistent with the results in Fig. 2.

After knowing the transverse evolution at $z = 0$ ($t = \tau$), we can obtain the temperature and velocity at arbitrary z for the Bjorken cylinder system by [26–28, 36]

$$T(t, \rho, z) = T(\tau, \rho, 0), \quad (38)$$

$$v_\rho(t, \rho, z) = v_\rho(\tau, \rho, 0) \frac{\tau}{t}, \quad v_z = \frac{z}{t}. \quad (39)$$

Then, we can calculate the two-pion HBT correlation functions by a simulation [31, 32].

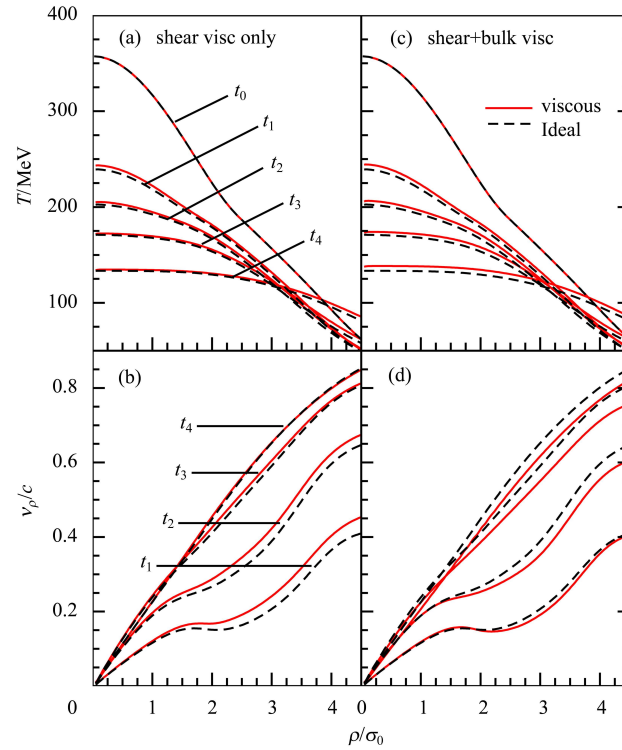


Fig. 2. (color online) The temperatures and transverse velocities of the viscous fluids with only shear viscosity ($C_s = 2$) and with the shear and bulk viscosities, in the $z = 0$ plane. The labeled time is respectively $t_0 = \tau_0$, $t_n = \tau_0 + 2^n(20\Delta\tau)$ ($n = 1, 2, 3, 4$, $\Delta\tau = 0.04$ fm/c).

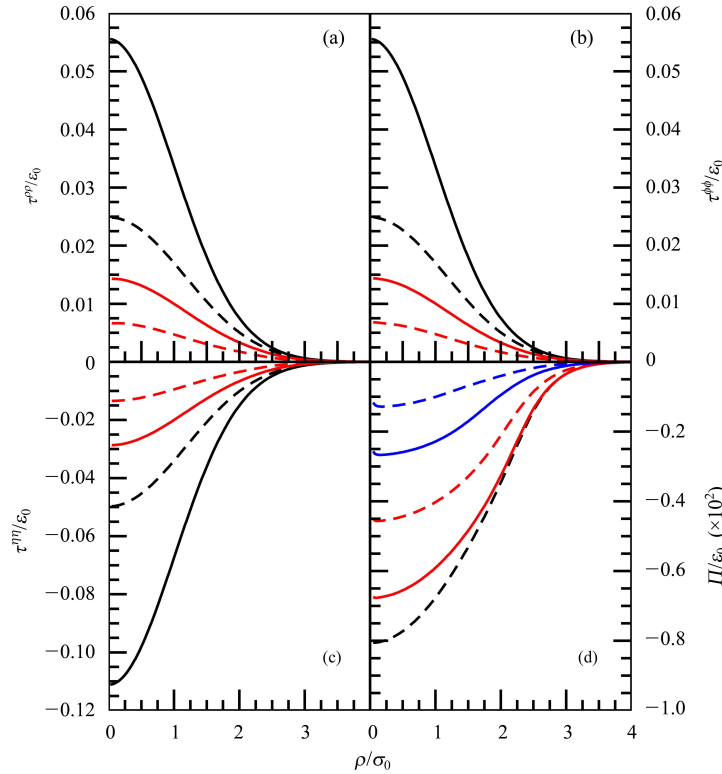


Fig. 3. (color online) The ratios of $\tau^{\rho\rho}$, $\tau^{\phi\phi}$, $\tau^{\eta\eta}$, and Π to ε_0 as functions of the transverse coordinate and time for the viscous fluid ($C_s = 2$). Here, the time is taken to be τ_0 (solid black), $\tau_0 + 6\Delta\tau$ (dashed black), $\tau_0 + 12\Delta\tau$ (solid red), $\tau_0 + 24\Delta\tau$ (dashed red), $\tau_0 + 48\Delta\tau$ (solid blue), and $\tau_0 + 96\Delta\tau$ (dashed blue), respectively. ($\Delta\tau = 0.04$ fm/c)

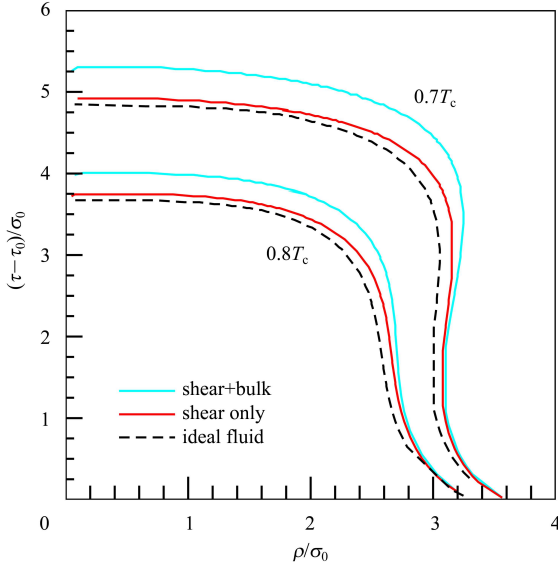


Fig. 4. (color online) The isotherms for 0.7 and 0.8 T_c in $z = 0$ plane.

4 Pion interferometry analysis

The two-pion HBT correlation function is defined as the ratio of the two-pion momentum distribution $P(k_1, k_2)$ to the product of the single-pion momentum distribution $P(k_1)P(k_2)$. For a chaotic pion-emitting source, $P(k_i)$ ($i = 1, 2$), and $P(k_1, k_2)$ can be expressed as [44]

$$P(k_i) = \sum_{X_i} A^2(k_i, X_i), \quad (40)$$

$$P(k_1, k_2) = \sum_{X_1, X_2} \left| \Phi(k_1, k_2; X_1, X_2) \right|^2, \quad (41)$$

where $A(k_i, X_i)$ is the magnitude of the amplitude for emitting a pion with 4-momentum $k_i = (\mathbf{k}_i, E_i)$ at X_i and $\Phi(k_1, k_2; X_1, X_2)$ is the two-pion wave function. Assuming that the emitted pions propagate as free

particles, $\Phi(k_1, k_2; X_1, X_2)$ is simply

$$\begin{aligned} \Phi(k_1, k_2; X_1, X_2) &= \frac{1}{\sqrt{2}} [A(k_1, X_1)A(k_2, X_2)e^{ik_1 \cdot X_1 + ik_2 \cdot X_2} \\ &+ A(k_1, X_2)A(k_2, X_1)e^{ik_1 \cdot X_2 + ik_2 \cdot X_1}]. \end{aligned} \quad (42)$$

For a set of variables of the relative momentum, $\{q_j\}$ ($q_j = |\mathbf{k}_1 - \mathbf{k}_2|_j$), the two-pion correlation function can be expressed as [32]

$$C(\{q_j\}) = \frac{\text{Cor}(\{q_j\})}{\text{Uncor}(\{q_j\})}, \quad (43)$$

where

$$\text{Cor}(\{q_j\}) = \int d\mathbf{k}_1 d\mathbf{k}_2 P(k_1, k_2) \prod_j \delta(|\mathbf{k}_1 - \mathbf{k}_2|_j - q_j) \quad (44)$$

and

$$\text{Uncor}(\{q_j\}) = \int d\mathbf{k}_1 d\mathbf{k}_2 P(k_1)P(k_2) \prod_j \delta(|\mathbf{k}_1 - \mathbf{k}_2|_j - q_j) \quad (45)$$

are the correlated and uncorrelated pion pair distributions with $\{q_j\}$.

In our simulated calculations, we first generate the pion momentum k on the freeze-out hypersurface $\Sigma(X)$ with temperature T_f , according to the probability of the Cooper-Frye formula [45]

$$P(k) \propto \int k^\mu d\Sigma_\mu f\left(\frac{k_\mu u^\mu}{T}\right). \quad (46)$$

For the viscous fluid, the distribution $f = f_0 + \delta f$. We take f_0 for the ideal fluid as the Boltzmann distribution, and take δf for the shear and bulk viscosities as [9]

$$\delta f = f_0 \left(\frac{k_\mu u^\mu}{T} \right) \frac{p^\mu p^\nu}{2(\varepsilon + p)T^2} \left(\pi_{\mu\nu} - \frac{2}{5} \Pi \Delta_{\mu\nu} \right). \quad (47)$$

In Cartesian frame, $\pi^{\mu\nu}$ can be expressed in terms of the cylindrical variables as [2]

$$\pi^{\mu\nu} = \begin{pmatrix} \Pi^{\rho\eta} \cosh^2 \eta - \tau^{\eta\eta} & \tau^{\rho\rho} \gamma^2 v_\rho \cos \phi \cosh \eta & \tau^{\rho\rho} \gamma^2 v_\rho \sin \phi \cosh \eta & \Pi^{\rho\eta} \cosh \eta \sinh \eta \\ \tau^{\rho\rho} \gamma^2 v_\rho \cos \phi \cosh \eta & \Pi^{\rho\phi} \cos^2 \phi + \tau^{\phi\phi} & \Pi^{\rho\phi} \cos \phi \sin \phi & \tau^{\rho\rho} \gamma^2 v_\rho \cos \phi \sinh \eta \\ \tau^{\rho\rho} \gamma^2 v_\rho \sin \phi \cosh \eta & \Pi^{\rho\phi} \cos \phi \sin \phi & \Pi^{\rho\phi} \sin^2 \phi + \tau^{\phi\phi} & \tau^{\rho\rho} \gamma^2 v_\rho \sin \phi \sinh \eta \\ \Pi^{\rho\eta} \cosh \eta \sinh \eta & \tau^{\rho\rho} \gamma^2 v_\rho \cos \phi \sinh \eta & \tau^{\rho\rho} \gamma^2 v_\rho \sin \phi \sinh \eta & \Pi^{\rho\eta} \cosh^2 \eta - \tau^{\rho\rho} \gamma^2 v_\rho^2 \end{pmatrix}, \quad (48)$$

where $\mu, \nu = t, x, y, z$, $\Pi^{\rho\eta} = \tau^{\rho\rho} \gamma^2 v_\rho^2 + \tau^{\eta\eta}$, and $\Pi^{\rho\phi} = \tau^{\rho\rho} \gamma^2 - \tau^{\phi\phi}$.

After obtaining the momenta k_i ($i = 1, 2$) of the pions emitted on the freeze-out hypersurface, we can construct the correlation functions for the variables

q_{out} , q_{side} , and q_{long} [33, 34], $C(q_{\text{out}}, q_{\text{side}}, q_{\text{long}})$, based on Eqs. (40)–(45), by summing over \mathbf{k}_1 and \mathbf{k}_2 for each $(q_{\text{out}}, q_{\text{side}}, q_{\text{long}})$ bin. Then, we extract the HBT radii R_{out} , R_{side} , and R_{long} by fitting the correlation function with the parametrized formula

$$C(q_{\text{out}}, q_{\text{side}}, q_{\text{long}}) = 1 + \lambda e^{-q_{\text{out}}^2 R_{\text{out}}^2 - q_{\text{side}}^2 R_{\text{side}}^2 - q_{\text{long}}^2 R_{\text{long}}^2}. \quad (49)$$

Figure 5 shows the HBT radii R_{out} , R_{side} , R_{long} , and λ parameter as functions of the transverse momentum of the pion pair, $k_T = |\mathbf{k}_{1T} + \mathbf{k}_{2T}|/2$, for the viscous and ideal hydrodynamic sources with the freeze-out temperatures 0.7 and 0.8 T_c . For the viscous sources, the parameter C_s is taken to be 2. For comparison, the RHIC experimental HBT results [46, 47] are also shown in the figure. It can be seen that the HBT radii for the lower freeze-out temperature are larger than those for the higher T_f . The viscosity increases the transverse HBT radii R_{out} and R_{side} for the source with the lower freeze-out temperature. By comparing with the experimental results, we find that the results of the longitudinal HBT radius R_{long} for the hydrodynamic sources with

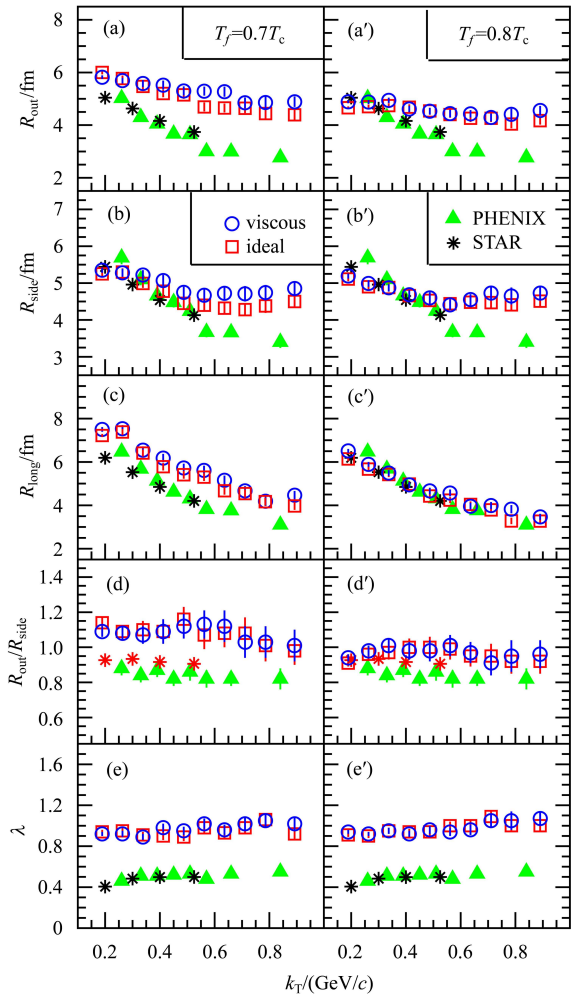


Fig. 5. (color online) The two-pion HBT results for the viscous ($C_s = 2$) and ideal hydrodynamic sources with $T_f = 0.7T_c$ and $T_f = 0.8T_c$. The experimental data are from the PHENIX [46] and STAR [47] collaborations.

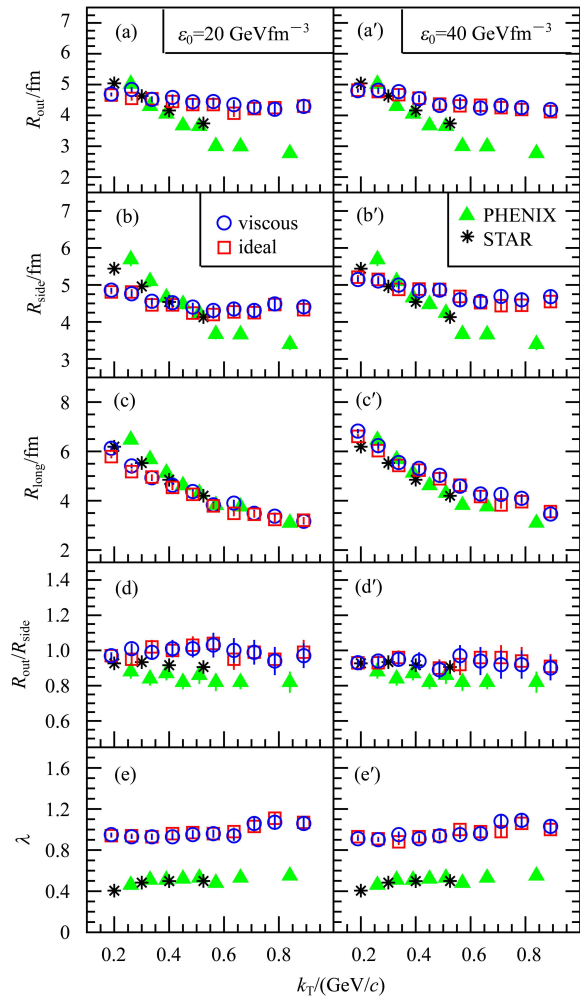


Fig. 6. (color online) The two-pion HBT results for the viscous ($C_s = 2$) and ideal hydrodynamic sources with $\epsilon_0 = 20 \text{ GeV/fm}^3$ and $\epsilon_0 = 40 \text{ GeV/fm}^3$. The freeze-out temperature is $0.8T_c$. The experimental data are from the PHENIX [46] and STAR [47] collaborations.

$T_f = 0.8T_c$ agree well with the experimental data. It indicates that the Bjorken scaling hypothesis is suitable in the description of the source longitudinal evolution. In our calculations, the width of the Bjorken rapidity plateau is taken to be 1.3. One can also see that the transverse HBT radii R_{out} and R_{side} as functions of k_T are flat for both of the two freeze-out temperatures. However, the ratio $R_{\text{out}}/R_{\text{side}}$ decreases to about one for the higher T_f . We did not consider the source coherence and the Coulomb interaction between the pions, so the λ results of the hydrodynamical sources are about unit.

In Table 1 we list the HBT results for the ideal and viscous hydrodynamical sources with $T_f = 0.8T_c$. Here the results of the ‘visc fluid 1’ and ‘visc fluid 2’ are for the viscous sources with only shear viscosity for $C_s = 1$ and $C_s = 2$. The results of the ‘visc fluid

Table 1. The HBT results for the ideal and viscous hydrodynamic sources with $T_f = 0.8T_c$.

$k_T/(\text{GeV}/c)$	sources	R_{out}/fm	$R_{\text{side}}/\text{fm}$	$R_{\text{long}}/\text{fm}$	$R_{\text{out}}/R_{\text{side}}$	λ
0.24	ideal fluid	4.69 ± 0.04	5.01 ± 0.04	5.89 ± 0.06	0.94 ± 0.02	0.91 ± 0.01
	visc fluid 1	4.72 ± 0.04	4.95 ± 0.04	5.96 ± 0.06	0.95 ± 0.02	0.92 ± 0.01
	visc fluid 2	4.80 ± 0.04	4.99 ± 0.04	5.98 ± 0.06	0.96 ± 0.02	0.93 ± 0.01
	visc fluid 3	4.82 ± 0.04	4.96 ± 0.05	6.00 ± 0.06	0.97 ± 0.02	0.92 ± 0.01
	visc fluid 4	4.89 ± 0.04	5.02 ± 0.05	6.16 ± 0.06	0.97 ± 0.02	0.93 ± 0.01
0.39	ideal fluid	4.68 ± 0.06	4.73 ± 0.07	5.06 ± 0.08	0.99 ± 0.03	0.93 ± 0.02
	visc fluid 1	4.63 ± 0.06	4.77 ± 0.07	4.91 ± 0.08	0.97 ± 0.03	0.92 ± 0.02
	visc fluid 2	4.66 ± 0.06	4.76 ± 0.06	4.85 ± 0.07	0.98 ± 0.03	0.91 ± 0.02
	visc fluid 3	4.67 ± 0.06	4.79 ± 0.07	4.95 ± 0.08	0.97 ± 0.03	0.91 ± 0.02
	visc fluid 4	4.77 ± 0.07	4.81 ± 0.07	5.09 ± 0.08	0.99 ± 0.03	0.90 ± 0.02
0.55	ideal fluid	4.46 ± 0.08	4.51 ± 0.08	4.38 ± 0.08	0.99 ± 0.03	0.95 ± 0.02
	visc fluid 1	4.45 ± 0.08	4.48 ± 0.08	4.28 ± 0.08	0.99 ± 0.04	0.95 ± 0.02
	visc fluid 2	4.49 ± 0.08	4.52 ± 0.08	4.17 ± 0.08	0.99 ± 0.04	0.94 ± 0.02
	visc fluid 3	4.49 ± 0.08	4.63 ± 0.09	4.40 ± 0.09	0.97 ± 0.04	0.90 ± 0.03
	visc fluid 4	4.52 ± 0.08	4.60 ± 0.09	4.48 ± 0.09	0.98 ± 0.04	0.92 ± 0.03
0.70	ideal fluid	4.25 ± 0.09	4.51 ± 0.10	3.88 ± 0.09	0.94 ± 0.04	0.98 ± 0.03
	visc fluid 1	4.23 ± 0.09	4.56 ± 0.10	3.92 ± 0.09	0.93 ± 0.04	0.99 ± 0.03
	visc fluid 2	4.23 ± 0.09	4.59 ± 0.10	3.78 ± 0.09	0.92 ± 0.04	0.95 ± 0.03
	visc fluid 3	4.26 ± 0.10	4.56 ± 0.11	3.91 ± 0.10	0.93 ± 0.04	0.95 ± 0.03
	visc fluid 4	4.30 ± 0.10	4.67 ± 0.11	3.89 ± 0.10	0.92 ± 0.04	0.94 ± 0.03
0.84	ideal fluid	4.23 ± 0.12	4.42 ± 0.13	3.37 ± 0.10	0.96 ± 0.05	0.97 ± 0.04
	visc fluid 1	4.24 ± 0.12	4.46 ± 0.12	3.43 ± 0.10	0.95 ± 0.05	0.97 ± 0.04
	visc fluid 2	4.32 ± 0.12	4.40 ± 0.12	3.59 ± 0.10	0.98 ± 0.05	1.01 ± 0.04
	visc fluid 3	4.44 ± 0.13	4.48 ± 0.13	3.60 ± 0.11	0.99 ± 0.06	1.02 ± 0.04
	visc fluid 4	4.77 ± 0.14	4.85 ± 0.15	3.67 ± 0.12	0.98 ± 0.06	1.05 ± 0.05

3' and 'visc fluid 4' are for the viscous sources with both the shear and bulk viscosities for $C_s = 1$ and $C_s = 2$. One can see that for the higher freeze-out temperature, the viscosity effect on the HBT results for the only shear viscous sources are negligible, and the viscosity effect for the source with both the shear and bulk viscosities may let the HBT radii be a little larger than those of the ideal fluid source.

Further, we examine the HBT radii for the viscous hydrodynamical sources with lower initial energy density ($\varepsilon_0 = 20 \text{ GeV}/\text{fm}^3$) and higher initial energy density ($\varepsilon_0 = 40 \text{ GeV}/\text{fm}^3$). The results are shown in Fig. 6, where the freeze-out temperature is $0.8T_c$. It can be seen that the results of the transverse HBT radius R_{side} for the higher initial energy density are larger than those for the lower initial energy density. This leads to the smaller values of the ratio $R_{\text{out}}/R_{\text{side}}$ for the source with higher ε_0 . The longitudinal HBT radius R_{long} also increases with the initial energy density. However, the transverse HBT radii as functions of the transverse momentum k_T are more flat than those of the experimental data, both for the lower and higher initial energy density sources.

5 Conclusion

Based on the Israel-Stewart second-order theory of relativistic dissipative fluid dynamics [23], we investigate the space-time evolution of the viscous hydrodynamics with the Bjorken cylinder geometry. The EOS used in the hydrodynamic calculations combines hadron resonance gas at low temperatures with lattice QCD at high temperatures [43]. We consider both the shear and bulk viscosities in the hydrodynamic evolution of the dissipative fluids. By performing the two-pion HBT interferometry to the viscous and ideal hydrodynamic sources, we investigate the effects of the viscosities on the two-pion HBT interferometry results.

For a dissipative fluid there is not only shear viscosity but also bulk viscosity. For the sQGP produced in relativistic heavy ion collisions [1], the ratio of the shear viscosity to the entropy density satisfies $\tilde{\eta}/s \gtrsim 1/4\pi$ [37–39], and the bulk viscosity $\tilde{\zeta}$ is proportional to $\tilde{\eta}(v_s^2 - 1/3)$ [17, 40–42]. Our calculations indicate that the viscosity effect on the two-pion HBT

results is small if only the shear viscosity is considered. The bulk viscosity leads to a larger transverse freeze-out configuration of the pion sources, and therefore increases the transverse HBT radii. This effect is larger if the source has a lower freeze-out temperature. In the present paper we took the relaxation time $\tau_\pi = \frac{6\tilde{\eta}}{sT}$ [6, 10, 12, 15, 23] and $\tau_\Pi = \tau_\pi$ [17, 18], and used an uniform formula of the shear viscosities for both the QGP and hadronic phases. We find that there are not observable influences on the viscosity effects on HBT results for the τ_π and τ_Π values within reasonable ranges. In Ref. [18] different viscosities for the QGP and hadronic phases are taken into account in the analyses of transverse momentum spectra, elliptic flow, and HBT interferometry. Further investigations of the effects of shear and bulk viscosities on the HBT interferometry for more realistic viscous pion-emitting sources in relativistic heavy ion collisions are of great interest in the future.

In our model the Bjorken longitudinal scaling hy-

pothesis [25] is adopted, which is an approximation for the heavy ion collisions at very high energies. Our results indicate that the longitudinal HBT radius for the Bjorken cylinder hydrodynamic source agrees well with the RHIC HBT results. However, the transverse HBT radii as functions of the pair transverse momentum for our Bjorken cylinder sources are flatter than those of the experimental data. In order to explain the RHIC HBT results, various models without viscosity were proposed [48–53]. Recently, the hydrodynamic source model including the initial collective flow, a stiffer EOS, and viscosity was proposed [54] to explain the RHIC HBT results. A comprehensive examination of the effects in these models on HBT interferometry and other observables (e.g. particle momentum distributions, elliptic flow, etc.) requires considerable effort.

The authors would like to thank Dr. S. Khakshur-nia for helpful discussions.

Appendix A

Derivation for relaxation equations

Here we give the derivations of Eqs. (24)–(26) from Eq. (22) in detail. For the Bjorken cylinder and at $z = 0$, we have

$$\pi^{\mu\nu} = \begin{pmatrix} \gamma^2 v_\rho^2 \tau^{\rho\rho} & \gamma^2 v_\rho \tau^{\rho\rho} & 0 & 0 \\ \gamma^2 v_\rho \tau^{\rho\rho} & \gamma^2 \tau^{\rho\rho} & 0 & 0 \\ 0 & 0 & \rho^{-2} \tau^{\phi\phi} & 0 \\ 0 & 0 & 0 & \tau^{-2} \tau^{\eta\eta} \end{pmatrix}, \quad (\text{A1})$$

$$\begin{aligned} \pi_{\alpha\beta} = g_{\alpha\mu} \pi^{\mu\nu} g_{\nu\beta} &= \begin{pmatrix} 1 & 0 & 0 & 0 \\ 0 & -1 & 0 & 0 \\ 0 & 0 & -\rho^2 & 0 \\ 0 & 0 & 0 & -\tau^2 \end{pmatrix} \begin{pmatrix} \gamma^2 v_\rho^2 \tau^{\rho\rho} & \gamma^2 v_\rho \tau^{\rho\rho} & 0 & 0 \\ \gamma^2 v_\rho \tau^{\rho\rho} & \gamma^2 \tau^{\rho\rho} & 0 & 0 \\ 0 & 0 & \rho^{-2} \tau^{\phi\phi} & 0 \\ 0 & 0 & 0 & \tau^{-2} \tau^{\eta\eta} \end{pmatrix} \begin{pmatrix} 1 & 0 & 0 & 0 \\ 0 & -1 & 0 & 0 \\ 0 & 0 & -\rho^2 & 0 \\ 0 & 0 & 0 & -\tau^2 \end{pmatrix} \\ &= \begin{pmatrix} \gamma^2 v_\rho^2 \tau^{\rho\rho} & \gamma^2 v_\rho \tau^{\rho\rho} & 0 & 0 \\ -\gamma^2 v_\rho \tau^{\rho\rho} & -\gamma^2 \tau^{\rho\rho} & 0 & 0 \\ 0 & 0 & -\tau^{\phi\phi} & 0 \\ 0 & 0 & 0 & -\tau^{\eta\eta} \end{pmatrix} \begin{pmatrix} 1 & 0 & 0 & 0 \\ 0 & -1 & 0 & 0 \\ 0 & 0 & -\rho^2 & 0 \\ 0 & 0 & 0 & -\tau^2 \end{pmatrix} \\ &= \begin{pmatrix} \gamma^2 v_\rho^2 \tau^{\rho\rho} & -\gamma^2 v_\rho \tau^{\rho\rho} & 0 & 0 \\ -\gamma^2 v_\rho \tau^{\rho\rho} & \gamma^2 \tau^{\rho\rho} & 0 & 0 \\ 0 & 0 & \rho^2 \tau^{\phi\phi} & 0 \\ 0 & 0 & 0 & \tau^2 \tau^{\eta\eta} \end{pmatrix}, \quad (\text{A2}) \end{aligned}$$

and

$$\begin{aligned} \pi_{\beta}^{\mu} = g^{\mu\alpha} \pi_{\alpha\beta} &= \begin{pmatrix} 1 & 0 & 0 & 0 \\ 0 & -1 & 0 & 0 \\ 0 & 0 & -1/\rho^2 & 0 \\ 0 & 0 & 0 & -1/\tau^2 \end{pmatrix} \begin{pmatrix} \gamma^2 v_{\rho}^2 \tau^{\rho\rho} & -\gamma^2 v_{\rho} \tau^{\rho\rho} & 0 & 0 \\ -\gamma^2 v_{\rho} \tau^{\rho\rho} & \gamma^2 \tau^{\rho\rho} & 0 & 0 \\ 0 & 0 & \rho^2 \tau^{\phi\phi} & 0 \\ 0 & 0 & 0 & \tau^2 \tau^{\eta\eta} \end{pmatrix} \\ &= \begin{pmatrix} \gamma^2 v_{\rho}^2 \tau^{\rho\rho} & -\gamma^2 v_{\rho} \tau^{\rho\rho} & 0 & 0 \\ \gamma^2 v_{\rho} \tau^{\rho\rho} & -\gamma^2 \tau^{\rho\rho} & 0 & 0 \\ 0 & 0 & -\tau^{\phi\phi} & 0 \\ 0 & 0 & 0 & -\tau^{\eta\eta} \end{pmatrix}. \end{aligned} \quad (\text{A3})$$

A.1 The first term of Eq. (22)

The first term of Eq. (22) can be expanded as

$$\begin{aligned} \tau_{\pi} \Delta^{\mu\alpha} \Delta^{\nu\beta} D\pi_{\alpha\beta} &= \tau_{\pi} (g^{\mu\alpha} - u^{\mu} u^{\alpha}) (g^{\nu\beta} - u^{\nu} u^{\beta}) D\pi_{\alpha\beta} \\ &= \tau_{\pi} g^{\mu\alpha} g^{\nu\beta} D\pi_{\alpha\beta} - \tau_{\pi} g^{\mu\alpha} u^{\nu} u^{\beta} D\pi_{\alpha\beta} \\ &\quad - \tau_{\pi} g^{\nu\beta} u^{\mu} u^{\alpha} D\pi_{\alpha\beta} \\ &\quad + \tau_{\pi} u^{\mu} u^{\alpha} u^{\nu} u^{\beta} D\pi_{\alpha\beta}. \end{aligned} \quad (\text{A4})$$

With the relations $Dg_{\kappa\beta} = Dg^{\kappa\beta} = 0$ and the orthogonality $u_{\mu} \pi^{\mu\nu} = u^{\mu} \pi_{\mu\nu} = 0$, we have

$$g^{\mu\alpha} g^{\nu\beta} D\pi_{\alpha\beta} = g^{\nu\beta} (Dg^{\mu\alpha} \pi_{\alpha\beta}) = g^{\nu\beta} D\pi_{\beta}^{\mu}, \quad (\text{A5})$$

$$\begin{aligned} g^{\mu\alpha} u^{\nu} u^{\beta} D\pi_{\alpha\beta} &= g^{\mu\alpha} u^{\nu} [(Du^{\beta} \pi_{\alpha\beta}) - (Du^{\beta}) \pi_{\alpha\beta}] \\ &= -g^{\mu\alpha} u^{\nu} (Du^{\beta}) \pi_{\alpha\beta}, \end{aligned} \quad (\text{A6})$$

$$\begin{aligned} g^{\nu\beta} u^{\mu} u^{\alpha} D\pi_{\alpha\beta} &= g^{\nu\beta} u^{\mu} [(Du^{\alpha} \pi_{\alpha\beta}) - (Du^{\alpha}) \pi_{\alpha\beta}] \\ &= -g^{\nu\beta} u^{\mu} (Du^{\alpha}) \pi_{\alpha\beta}, \end{aligned} \quad (\text{A7})$$

$$\begin{aligned} u^{\mu} u^{\nu} u^{\alpha} u^{\beta} D\pi_{\alpha\beta} &= u^{\mu} u^{\nu} [u^{\alpha} (Du^{\beta} \pi_{\alpha\beta}) \\ &\quad - (Du^{\beta}) u^{\alpha} \pi_{\alpha\beta}] = 0. \end{aligned} \quad (\text{A8})$$

So, the first term of Eq. (22) can be expressed as

$$\tau_{\pi} \Delta^{\mu\alpha} \Delta^{\nu\beta} D\pi_{\alpha\beta} = \tau_{\pi} (g^{\nu\beta} D\pi_{\beta}^{\mu} + I^{\mu\nu}), \quad (\text{A9})$$

where

$$I^{\mu\nu} \equiv g^{\mu\alpha} u^{\nu} (Du^{\beta}) \pi_{\alpha\beta} + g^{\nu\beta} u^{\mu} (Du^{\alpha}) \pi_{\alpha\beta}. \quad (\text{A10})$$

For the azimuth-symmetric Bjorken cylinder, $u^{\phi} = 0$ and $u^{\eta} = 0$ at $z = 0$, so $I^{\phi\phi} = I^{\eta\eta} = 0$.

Therefore, for $\mu = \nu = \rho$ we have

$$\begin{aligned} \Delta^{\mu\alpha} \Delta^{\nu\beta} D\pi_{\alpha\beta} &= g^{\rho\beta} D\pi_{\beta}^{\rho} + I^{\rho\rho} = D\gamma^2 \tau^{\rho\rho} \\ &\quad + I^{\rho\rho} = \gamma^3 \left(\frac{\partial}{\partial \tau} \tau^{\rho\rho} + v_{\rho} \frac{\partial}{\partial \rho} \tau^{\rho\rho} \right) \\ &\quad + 2\gamma (D\gamma) \tau^{\rho\rho} + I^{\rho\rho}, \end{aligned} \quad (\text{A11})$$

where

$$\begin{aligned} I^{\rho\rho} &= g^{\rho\alpha} u^{\rho} (Du^{\beta}) \pi_{\alpha\beta} + g^{\rho\beta} u^{\rho} (Du^{\alpha}) \pi_{\alpha\beta} \\ &= g^{\rho\alpha} u^{\rho} (Du^{\beta}) \pi_{\alpha\beta} + g^{\rho\alpha} u^{\rho} (Du^{\beta}) \pi_{\beta\alpha} \\ &= 2g^{\rho\alpha} u^{\rho} (Du^{\beta}) \pi_{\alpha\beta} = 2g^{\rho\rho} u^{\rho} (Du^{\beta}) \pi_{\rho\beta} \\ &= -2u^{\rho} [(D\gamma) \pi_{\rho\tau} + (D\gamma v_{\rho}) \pi_{\rho\rho}] \\ &= -2\gamma v_{\rho} [-(D\gamma) \gamma^2 v_{\rho} \tau^{\rho\rho} + (D\gamma v_{\rho}) \gamma^2 \tau^{\rho\rho}] \\ &= -2\gamma^4 v_{\rho} \tau^{\rho\rho} (Dv_{\rho}). \end{aligned} \quad (\text{A12})$$

With the relations,

$$\gamma = \frac{1}{\sqrt{1-v_{\rho}^2}}, \quad v_{\rho} \frac{\partial(\gamma v_{\rho})}{\partial \tau} = \frac{\partial \gamma}{\partial \tau}, \quad v_{\rho} \frac{\partial(\gamma v_{\rho})}{\partial \rho} = \frac{\partial \gamma}{\partial \rho}, \quad (\text{A13})$$

we have

$$\begin{aligned} I^{\rho\rho} &= -2\gamma^3 \tau^{\rho\rho} [v_{\rho} (D\gamma v_{\rho}) - v_{\rho}^2 (D\gamma)] \\ &= -2\gamma^3 \tau^{\rho\rho} \left[v_{\rho} \gamma \left(\frac{\partial(\gamma v_{\rho})}{\partial \tau} + v_{\rho} \frac{\partial(\gamma v_{\rho})}{\partial \rho} \right) - v_{\rho}^2 (D\gamma) \right] \\ &= -2\gamma^3 \tau^{\rho\rho} \left[\gamma \left(\frac{\partial \gamma}{\partial \tau} + v_{\rho} \frac{\partial \gamma}{\partial \rho} \right) - v_{\rho}^2 (D\gamma) \right] \\ &= -2\gamma \tau^{\rho\rho} D\gamma, \end{aligned} \quad (\text{A14})$$

and

$$\Delta^{\mu\alpha} \Delta^{\nu\beta} D\pi_{\alpha\beta} = \gamma^3 \left(\frac{\partial}{\partial \tau} \tau^{\rho\rho} + v_{\rho} \frac{\partial}{\partial \rho} \tau^{\rho\rho} \right), \quad (\text{A15})$$

for $\mu = \nu = \rho$.

For $\mu = \nu = \phi$ and $\mu = \nu = \eta$, we have

$$\Delta^{\mu\alpha} \Delta^{\nu\beta} D\pi_{\alpha\beta} = \frac{1}{\rho^2} D\tau^{\phi\phi} = \frac{\gamma}{\rho^2} \left(\frac{\partial}{\partial \tau} \tau^{\phi\phi} + v_{\rho} \frac{\partial}{\partial \rho} \tau^{\phi\phi} \right), \quad (\text{A16})$$

and

$$\Delta^{\mu\alpha}\Delta^{\nu\beta}D\pi_{\alpha\beta} = \frac{1}{\tau^2}D\tau^{\phi\phi} = \frac{\gamma}{\tau^2}\left(\frac{\partial}{\partial\tau}\tau^{\eta\eta} + v_\rho\frac{\partial}{\partial\rho}\tau^{\eta\eta}\right). \quad (\text{A17})$$

A.2 The third term of Eq. (22)

For the third term of Eq. (22), we have

$$\begin{aligned} \nabla^{\langle\mu}u^{\nu\rangle} &\equiv \nabla^{\langle\mu}u^{\nu\rangle} - \frac{1}{3}\Delta^{\mu\nu}d_\lambda u^\lambda \\ &= \left[\frac{\nabla^\mu u^\nu + \nabla^\nu u^\mu}{2}\right] - \frac{1}{3}\Delta^{\mu\nu}\Theta. \end{aligned} \quad (\text{A18})$$

With the relations

$$v_\rho\frac{\partial(\gamma v_\rho)}{\partial\tau} = \frac{\partial\gamma}{\partial\tau}, \quad \frac{\partial(\gamma v_\rho)}{\partial\rho} = \frac{1}{v_\rho}\frac{\partial\gamma}{\partial\rho}, \quad (\text{A19})$$

we have

$$\nabla^\rho u^\rho = -\gamma^2\left[\frac{\partial\gamma}{\partial\tau} + \frac{\partial(\gamma v_\rho)}{\partial\rho}\right] \equiv -\gamma^2\theta, \quad (\text{A20})$$

and

$$\nabla^{\langle\rho}u^{\rho\rangle} = \gamma^2\left(-\theta + \frac{1}{3}\Theta\right) = \gamma^2\sigma^{\rho\rho}, \quad (\text{A21})$$

where

$$\theta = \frac{\partial\gamma}{\partial\tau} + \frac{\partial(\gamma v_\rho)}{\partial\rho}. \quad (\text{A22})$$

Similarly, we have

$$\nabla^\phi u^\phi = \frac{1}{\rho^2}\left(\frac{-\gamma v_\rho}{\rho}\right), \quad (\text{A23})$$

$$\nabla^{\langle\phi}u^{\phi\rangle} = \frac{1}{\rho^2}\left(\frac{-\gamma v_\rho}{\rho} + \frac{1}{3}\Theta\right) = \frac{1}{\rho^2}\sigma^{\phi\phi}, \quad (\text{A24})$$

$$\nabla^\eta u^\eta = \frac{1}{\tau^2}\left(\frac{-\gamma}{\tau}\right), \quad (\text{A25})$$

$$\nabla^{\langle\eta}u^{\eta\rangle} = \frac{1}{\tau^2}\left(\frac{-\gamma}{\tau} + \frac{1}{3}\Theta\right) = \frac{1}{\tau^2}\sigma^{\eta\eta}, \quad (\text{A26})$$

$$\nabla^\tau u^\tau = -\gamma^2 v_\rho^2\left(\frac{\partial\gamma}{\partial\tau} + \frac{\partial\gamma v_\rho^2}{\partial\rho}\right) = -\gamma^2 v_\rho^2\theta, \quad (\text{A27})$$

$$\nabla^{\langle\tau}u^{\tau\rangle} = \gamma^2 v_\rho^2\left(-\theta + \frac{1}{3}\Theta\right) = \gamma^2 v_\rho^2\sigma^{\tau\tau}, \quad (\text{A28})$$

$$\nabla^\tau u^\rho = \nabla^\rho u^\tau = -\gamma^2 v_\rho\theta, \quad (\text{A29})$$

$$\begin{aligned} \nabla^{\langle\tau}u^{\rho\rangle} &= \nabla^{\langle\rho}u^{\tau\rangle} = \gamma^2 v_\rho\left(-\theta + \frac{1}{3}\Theta\right) \\ &= \gamma^2 v_\rho\sigma^{\tau\rho}. \end{aligned} \quad (\text{A30})$$

A.3 The last term of Eq. (22)

The last term of Eq. (22) can be written as

$$\begin{aligned} \tilde{\eta}Td_\lambda\left(\frac{\tau_\pi u^\lambda}{\tilde{\eta}}T\right) &= \tilde{\eta}T\left[\frac{\tau_\pi}{\tilde{\eta}T}d_\lambda u^\lambda + u^\lambda d_\lambda\left(\frac{\tau_\pi}{\tilde{\eta}T}\right)\right] \\ &= \tau_\pi\Theta + \tilde{\eta}TD\left(\frac{\tau_\pi}{\tilde{\eta}T}\right). \end{aligned} \quad (\text{A31})$$

Now, one can obtain Eqs. (24)–(26) from the above derivations.

References

- 1 Arsene I et al. (BRAHMS collaboration). Nucl. Phys. A, 2005, **757**: 1; Back B B et al. (PHOBOS collaboration). Nucl. Phys. A, 2005, **757**: 28; Adcox K et al. (STAR collaboration). Nucl. Phys. A, 2005, **757**: 102; Adams J et al. (PHENIX collaboration). Nucl. Phys. A, 2005, **757**: 184
- 2 Muronga A, Rischke D H. nucl-th/0407114
- 3 Heinz U, SONG H, Chaudhuri A K. Phys. Rev. C, 2006, **73**: 034904
- 4 Baier R, Romatschke P, Wiedemann U A. Phys. Rev. C, 2006, **73**: 064903; Baier R, Romatschke P. Eur. Phys. J. C, 2007, **51**: 677
- 5 Chaudhuri A K. Phys. Rev. C, 2006, **74**: 044904
- 6 Romatschke P. Eur. Phys. J. C, 2007, **52**: 203
- 7 Romatschke P, Romatschke U. Phys. Rev. Lett., 2007, **99**: 172301
- 8 Muronga A. Phys. Rev. C, 2007, **76**: 014909
- 9 Dusling K, Teaney D. Phys. Rev. C, 2008, **77**: 034905
- 10 SONG H, Heinz U. Phys. Lett. B, 2008, **658**: 279
- 11 SONG H, Heinz U. Phys. Rev. C, 2008, **77**: 064901
- 12 SONG H, Heinz U. Phys. Rev. C, 2008, **78**: 024902
- 13 Luzum M, Romatschke P. Phys. Rev. C, 2008, **78**: 034915; 2009, **79**: 039903
- 14 Luzum M, Romatschke P. Phys. Rev. Lett., 2009, **103**: 262302
- 15 Chaudhuri A K. Phys. Lett. B, 2009, **672**: 126; 2009, **681**: 418
- 16 Monnai A, Hirano T. Phys. Rev. C, 2009, **80**: 054906
- 17 SONG H, Heinz U. Phys. Rev. C, 2010, **81**: 024905
- 18 Bozek P. Phys. Rev. C, 2010, **81**: 034909
- 19 LI J W, MA Y G, MA G L. Chin. Phys. B, 2009, **18**: 3786
- 20 Eckart C. Phys. Rev., 1940, **58**: 919
- 21 Landau L D, Lifshitz, E M. Fluid Mechanics (Addison-Wesley, Massachusetts, 1959. 505
- 22 Müller I. Z. Phys., 1967, **198**: 329
- 23 Israel W. Ann. Phys., 1976, **100**: 310; Stewart J M. Proc. Roy. Soc. A, 1977, **357**: 59; Israel W, Stewart J M. Ann. Phys., 1979, **118**: 341
- 24 Muronga A. Phys. Rev. Lett., 2002, **88**: 062302; **89**: 159901; Phys. Rev. C, 2004, **69**: 034903
- 25 Bjorken J D. Phys. Rev. D, 1983, **27**: 140

- 26 Baym G, Friman B L, Blazot J P et al. Nucl. Phys. A, 1983, **407**: 541
- 27 Rischke D H, Gyulassy M. Nucl. Phys. A, 1996, **608**: 479
- 28 Efaaf M J, ZHANG W N, Khaliliyar M et al. HEP & NP, 2005, **29**: 467 (in Chinese)
- 29 Schneider A V et al. J. Comput. Phys., 1993, **105**: 92; Harten A, Lax P D, Leer B van. SIAM Rev., 1983, **25**: 35; Einfeldt B. SIAM J. Numer. Anal., 1988, **25**: 294
- 30 Rischke D H, Bernard S, Maruhn J A. Nucl. Phys. A, 1995, **595**: 346; Rischke D H. nucl-th/9809044
- 31 ZHANG W N, Efaaf M J, WONG C Y. Phys. Rev. C, 2004, **70**: 024903
- 32 ZHANG W N, LIU Y M, WANG S et al. Phys. Rev. C, 1993, **47**: 795; ZHANG W N, LIU Y M, HUO L et al. Phys. Rev. C, 1995, **51**: 922; ZHANG W N, TANG G X, CHEN X J et al. Phys. Rev. C, 2000, **62**: 044903
- 33 Bertsch G, GONG M, Tohyama M. Phys. Rev. C, 1988, **37**: 1896; Bertsch G. Nucl. Phys. A, 1989, **498**: 173c
- 34 Pratt S, Csörgő T, Zimányi J. Phys. Rev. C, 1990, **42**: 2646
- 35 SONG H. Causal Viscous Hydrodynamics for Relativistic Heavy Ion Collisions (Ph.D. Thesis), Ohio: Ohio State University, 2009; arXiv:0908.3656
- 36 ZHANG W N, YANG Z T, REN Y Y. Phys. Rev. C, 2009, **80**: 044908
- 37 Kovtun P, Son D T, Starinets A O. JHEP, 2003, **0310**: 064
- 38 Buchel A, LIU J T. Phys. Rev. Lett., 2004, **93**: 090602
- 39 Kovtun P, Son D T, Starinets A O. Phys. Rev. Lett., 2005, **94**: 111601
- 40 Benincasa P, Buchel A, Starinets A O. Nucl. Phys. B, 2006, **733**: 160
- 41 Buchel A. Phys. Rev. D, 2005, **72**: 106002
- 42 Buchel A. Phys. Lett. B, 2008, **663**: 286; Buchel A, Pagnutti C. Nucl. Phys. B, 2009, **816**: 62
- 43 Huovinen P, Petreczky P. Nucl. Phys. A, 2010, **837**: 26
- 44 WONG C Y. Introduction to High-Energy Heavy-Ion Collisions. Singapore: World Scientific, 1994: Chap. 17
- 45 Cooper F, Frye G. Phys. Rev. D, 1974, **10**: 186
- 46 Adler S S et al. (PHENIX collaboration). Phys. Rev. Lett., 2004, **93**: 152302
- 47 Adams J et al. (STAR collaboration). Phys. Rev. C, 2005, **71**: 044906
- 48 LIN Z, KO C M, Pal S. Phys. Rev. Lett., 2002, **89**: 152301
- 49 Socolowski Jr O, Grassi F, Hama Y et al. Phys. Rev. Lett., 2004, **93**: 182301
- 50 ZHANG W N, REN Y Y, WONG C Y. Phys. Rev. C, 2006, **74**: 024908
- 51 Cramer J G, Miller G A, WU J M S et al. Phys. Rev. Lett., 2005, **94**: 102302
- 52 Frodermann E, Heinz U, Lisa M A. Phys. Rev. C, 2006, **73**: 044908
- 53 Broniowski W, Chojnacki M, Florkowski W et al. Phys. Rev. Lett., 2008, **101**: 022301
- 54 Pratt S. Phys. Rev. Lett., 2009, **102**: 232301